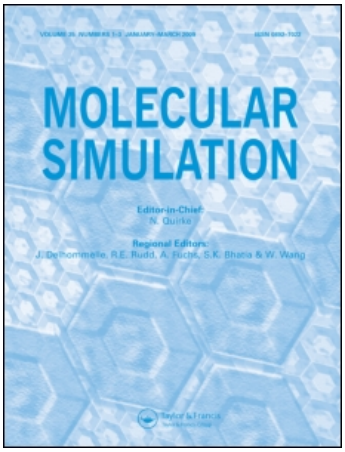

Molecular Simulation
Publication details, including instructions for authors and subscription information:
http://www.informaworld.com/smpp/title~content=t713644482

On the factors affecting tautomerism: consequences of N-substituents (Me/NR_2) in structures derived from salicylaldimines

Tareq Irshaidat[a]
[a] Department of Chemistry, College of Sciences, Al-Hussein Bin Talal University, Ma'an, Jordan

First published on: 29 July 2009

To cite this Article Irshaidat, Tareq(2010) 'On the factors affecting tautomerism: consequences of N-substituents (Me/NR_2) in structures derived from salicylaldimines', Molecular Simulation, 36: 1, 41 — 52, First published on: 29 July 2009 (iFirst)
To link to this Article: DOI: 10.1080/08927020903096080
URL: http://dx.doi.org/10.1080/08927020903096080

Molecular Simulation
Vol. 36, No. 1, January 2010, 41–52

Taylor & Francis
Taylor & Francis Group

On the factors affecting tautomerism: consequences of N-substituents (Me/NR_2) in structures derived from salicylaldimines

Tareq Irshaidat*

Department of Chemistry, College of Sciences, Al-Hussein Bin Talal University, Ma'an, Jordan

(*Received 7 April 2009; final version received 28 May 2009*)

This computational organic chemistry study was performed using the B3LYP and the Hartree–Fock methods. Other methods were compared using two model compounds, and these methods are: second-order Møller–Plesset, fourth-order Møller–Plesset, quadratic configuration interaction with single and double excitation and coupled cluster single and double excitations. The study included discussions of the following aspects: the molecular structures, the harmonic oscillator measure of aromaticity, the energy differences between the tautomers, selected infrared stretching frequencies, the atomic charges (Mulliken and natural population analysis), selected NMR chemical shifts, the molecular orbital diagrams and the R groups. The calculations revealed that the electronic structure of salicylaldimines is sensitive to this substitution and may change the physical organic aspects including tautomerism significantly. The results illustrate that the proton–electron delocalisation as a sub-molecular event might be a controllable process when a powerful H-bond exists. This is a new discovery in the area of tautomerism-based functional materials that will help in fine-tuning their properties.

Keywords: DFT; Hartree–Fock; tautomerism; hydrazine methylidenes; Schiff bases

1. Introduction

One of the known families of the applied molecular materials is Schiff bases derived from salicylaldehydes. This family of compounds is known in many technological applications; photochromism and thermochromism applications [1–5], as molecular electronic devices [6,7], as optical switches [8], as photodetectors [9] and in photodynamic cancer therapy [10]. These applications, at the molecular level, depend on the ability of Schiff bases to tautomerise; to exist as the keto-enamine and the enol-imine tautomers with small energy required for the proton–electron delocalisation [1].

The hydrazines derived from salicylaldehydes are another interesting group of compounds; a wide range of derivatives can be prepared by simple condensation procedures. In addition to that, they are stable on shelf and resist the humidity and the atmospheric oxygen, which are desirable properties for potential molecular materials. Despite that, tautomerism and the molecular characteristics of these compounds have received much less attention [1] than the Schiff bases [11,12], therefore, we devoted this theoretical work to study how changing the N-substituent from carbon (methyl group) to NR_2 would affect the tautomerism process and other physical organic aspects (see Figure 1 for the main idea). The structures are presented in Figure 2 (**H-1**, **H-2**, **DH-1**, **DH-2**, **SB-1** and **SB-2**). The six systems were compared based on (a) the geometry; the molecular structure parameters and the harmonic oscillator measure of aromaticity (HOMA), (b) the energy difference between the tautomers of each system (c) the atomic charges, (d) the infrared stretching frequencies, (e) the NMR chemical shifts (^{1}H, ^{13}C and ^{15}N) and (f) the molecular orbital diagrams which were used to gain an insight about the intramolecular electron densities interactions that are essential in determining the stability of the keto-tautomers of **H-1**, **H-2**, **DH-1** and **DH-2**.

2. Methods

The aromaticity index HOMA [13–15] is a method that employs values of the bond lengths to estimate the p-orbitals overlapping and the π-electrons delocalisation. For example, if we consider the conjugated cyclic system C_6H_6, the Kekulé structure has a HOMA value $= 0$, while HOMA $= 1$ indicates that the double bonds are fully delocalised, which is the known benzene ring. Values of HOMA < 1 and > 0 are the most common. Our previous studies [11,12] showed that in push–pull systems, as in Schiff bases and the analogous hydrazines, the higher HOMA values mean easier charge separation and better conduction at the molecular level. This allows to predict, on a comparative basis, changes in the electron density distribution.

All the geometries were optimised using B3LYP/6-31G(d) [16–18], as implemented in Gaussian 03 [19]. The basis set 6-31G(d) is a good basis set and can produce an acceptable HOMA value for benzene; 0.98, while other

*Email: tirshaidat@yahoo.com

ISSN 0892-7022 print/ISSN 1029-0435 online

DOI: 10.1080/08927020903096080
http://www.informaworld.com

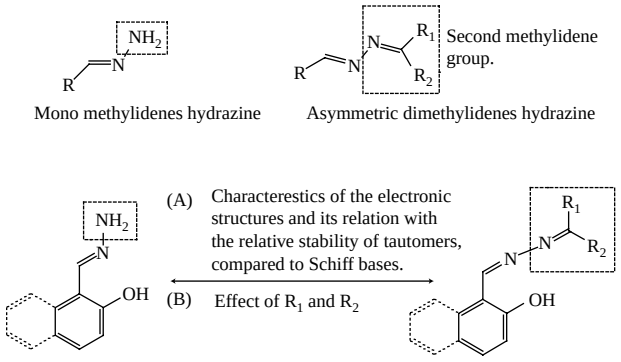

Figure 1. The main idea of this study.

basis sets and methods do not improve the geometry significantly. The atomic charges were calculated through two schemes, the natural population analysis charges (NPA) [20] and Mulliken charges [21]. The zero number of the imaginary frequencies for each optimised geometry indicated that they are minima. The simplest OCCCN tautomerism systems (Figure 3) were used to compare different computational procedures (Tables 1 and 2). Tables 1 and 2 include results from full optimisations and single point calculations from other common methods; HF [22], second-order Møller–Plesset (MP2) [23], fourth-order Møller–Plesset (MP4) [24], quadratic configuration interaction with single and double excitation (QCISD) [25] and coupled cluster single and double excitations (CCSD) [26], and using other basis sets; 3-21G(d) [27] and 6-311 ++G(d,p) [28]. The NMR chemical shifts presented in Table 9 were calculated by employing the gauge invariant atomic orbital [29] method using B3LYP/6-311+G(2d,p)//B3LYP/6-31G(d). The reference for the ^{1}H and the ^{13}C spectra is tetramethylsilane, and for ^{15}N is ammonia. The molecular orbital calculations are based on the B3LYP/6-31G(d) calculations. The small letters 'a' and 'b' accompanying symbols of the structures refer to the enol- and the keto-tautomers, respectively.

3. Results and discussion

3.1 Evaluation of the computational procedure

Two model structures were selected (Figure 3, **MH** and **MSB**) to evaluate the performance of a variety of computational procedures (Tables 1 and 2). The accuracies were compared based on the HOMA and the ΔE values. The obtained results from CCSD/6-31G(d) represent acceptable qualitative reference value because the principal purpose is finding a practical method (time vs. accuracy) to establish qualitative comparison among the structures not calculating absolute numbers. The absolute difference (AD) for the other procedures was calculated according to $\mathrm{AD} = |\Delta E_{\mathrm{CCSD/6\text{-}31G(d)}} - \Delta E_{\mathrm{other}}|$.

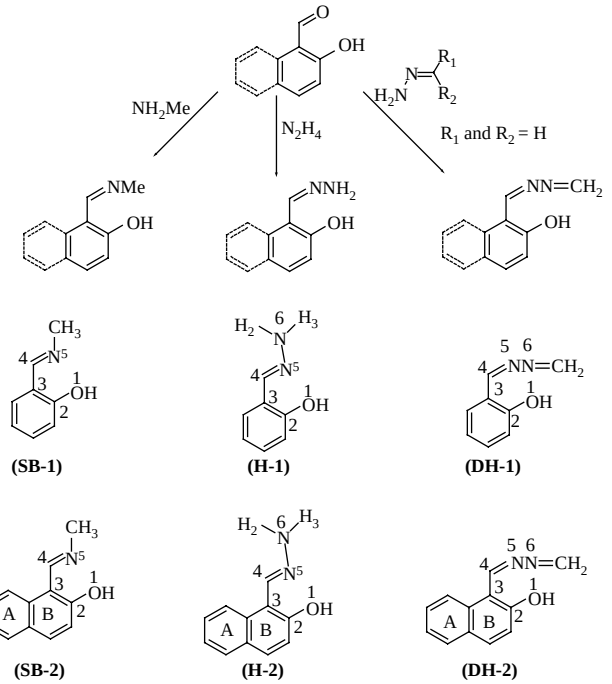

Figure 2. Structures of the mono- and the dimethylidene hydrazines derived from salicylaldehyde and 2-hydroxy-1-naphthaldehyde and the Schiff bases used for the comparison.

The entries 6, 8, 10, 12, 21, 23 (Table 1; **MH**) present the best ΔE results (the lowest AD values) obtained by computational procedures based on the HF and the MP4 methods. The methods are arranged according to their accuracy as the following: HF and MP4 > B3LYP > MP2. The computational procedure HF/3-21G(d) (AD = 0.33) is the most practical (time and accuracy).

In the light of the acceptable performance of the HF method in calculating the ΔE of **MH**, evaluating the computational procedures was narrowed down for **MSB** (Table 2). The entries 1, 3, 6, 8 and 9 (Table 2) show that the HF method performed well with respect to the reference value obtained from CCSD/6-31G(d), and the HF/3-21G(d) seems again to be a practical procedure

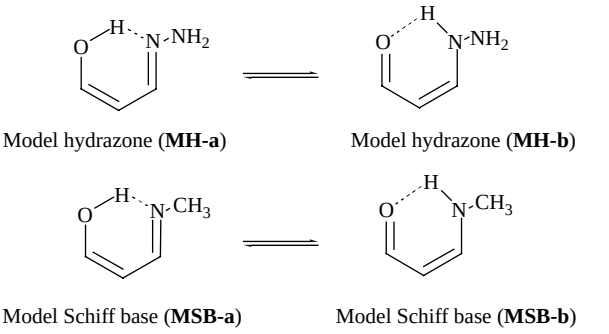

Figure 3. The OCCCN structures used to evaluate a variety of computational procedures in Tables 1 and 2.

Table 1. The HOMA, the ΔE (kcal/mol) and the AD[a] values for MH (Figure 3).

	MH			
Entry	Calculation type	HOMA	ΔE	AD
1	B3LYP/3-21G(d)	0.87	−2.96	3.04
2	B3LYP/6-31G(d)//B3LYP/3-21G(d)	–	−2.94	3.06
3	HF/6-31G(d)//B3LYP/3-21G(d)	–	−8.81	2.81
4	MP2/6-31G(d)//B3LYP/3-21G(d)	–	−1.84	4.16
5	MP4/6-31G(d)//B3LYP/3-21G(d)	–	−8.82	2.82
6	HF/3-21G(d)	0.71	−6.33	0.33
7	B3LYP/6-31G(d)//HF/3-21G(d)	–	−3.33	2.67
8	HF/6-31G(d)//HF/3-21G(d)	–	−6.28	0.28
9	MP2/6-31G(d)//HF/3-21G(d)	–	−1.61	4.39
10	MP4/6-31G(d)//HF/3-21G(d)	–	−6.29	0.29
11	B3LYP/6-31G(d)	0.79	−2.09	3.91
12	HF/6-31G(d)	0.57	−5.64	0.36
13	B3LYP/6-311 ++G(d,p)	0.79	−1.02	4.98
14	MP2/6-31G(d)	0.81	−0.68	5.32
15	HF/6-311 ++G(d,p)	0.55	−4.10	1.9
16	B3LYP/6-311 ++G(d,p)//B3LYP/6-31G(d)	–	−1.07	4.93
17	B3LYP/6-311 + G(2d,p)//B3LYP/6-31G(d)	–	−0.92	5.08
18	MP2/6-31G(d)//B3LYP/6-31G(d)	–	−0.59	5.41
19	HF/6-311 ++G(d,p)//B3LYP/6-31G(d)	–	−4.65	1.35
20	MP2/6-311 ++G(d,p)//B3LYP/6-31G(d)	–	+1.40	4.6
21	MP4/6-31G(d)//B3LYP/6-31G(d)	–	−6.23	0.23
22	CCSD/6-31G(d)	0.72	−6.00	0.00
23	CCSD/6-31G(d)//B3LYP/6-31G(d)	–	−6.26	0.26
24	QCISD/6-31G(d)//B3LYP/6-31G(d)	–	−6.90	0.90

[a] $AD = |\Delta E_{CCSD/6\text{-}31G(d)} - \Delta E_{other}|$.

(AD = 1.31). Accuracy of the methods is arranged as the following: HF and MP4 > B3LYP > MP2, which is the same trend obtained for **MH**. Both the accuracy and the computations time are equally important, hence, for relatively larger systems the most practical method for computing the ΔE is HF/3-21G(d). The reader should be aware that this is not a generalisation but this order is qualitatively valid only to calculate the energy of the tautomerism process. However, estimating ΔE using HF/3-21G(d) (solvent)//HF/3-21G(d) (gas phase) produced a value very comparable to the experimental value (Section 3.9). This example supports further that HF/3-21G(d) might be used to estimate qualitatively the energy of tautomerism. Unfortunately and to best of our knowledge, the literature does not include experimental information in this regard for comparison.

Table 2. The HOMA, the ΔE (kcal/mol) and the AD values for MSB (Figure 3).

	MSB			
Entry	Computational procedure	HOMA	ΔE	AD
1	HF/3-21G(d)	0.78	−10.10	1.31
2	B3LYP/3-21G(d)	–	–[a]	–
3	HF/6-31G(d)	0.64	−8.77	0.02
4	B3LYP/6-31G(d)	0.84	−7.55	1.24
5	MP2/6-31G(d)	0.86	−5.90	2.89
6	HF/6-311 ++G(d,p)	0.62	−7.34	1.45
7	B3LYP/6-311 ++G(d,p)	0.85	−6.73	2.06
8	HF/6-31G(d)//B3LYP/6-31G(d)	–	−9.66	0.87
9	HF/6-311 ++G(d,p)//B3LYP/6-31G(d)	–	−8.20	0.59
10	MP2/6-31G(d)//B3LYP/6-31G(d)	–	−5.98	2.81
11	MP4/6-31G(d)//B3LYP/6-31G(d)	–	−9.66	0.87
12	QCISD/6-31G(d)//B3LYP/6-31G(d)	–	−9.66	0.87
13	CCSD/6-31G(d)/B3LYP/6-31G(d)	–	−9.66	0.87
14	CCSD/6-31G(d)	0.84	−8.79	0.00

[a] $AD = |\Delta E_{CCSD/6\text{-}31G(d)} - \Delta E_{other}|$.

Table 3. Selected structural parameters for the enol tautomer of the six structures (Figure 2).

Parameter	**SB-1**	**SB-2**	**H-1**	**H-2**	**DH-1**	**DH-2**
O1—H1	0.999	1.008	0.989	0.994	0.995	1.003
N5—H1	1.743	1.665	1.796	1.728	1.771	1.697
O1—C2	1.343	1.337	1.349	1.345	1.342	1.337
C2—C3	1.422	1.410	1.421	1.407	1.424	1.413
C3—C4	1.456	1.454	1.456	1.456	1.446	1.443
C4—N5	1.284	1.289	1.289	1.292	1.296	1.301
H1—O1—C2	107.2	107.1	107.9	108.0	108.0	108.0
H2—N6—N5	–	–	113.3	113.0	–	–
H3—N6—N5	–	–	109.1	109.0	–	–
H3—N6—N5—C4	–	–	151.6	151.1	–	–

In general, when calculating physical properties (infrared frequencies, atomic charges, NMR chemical shifts and molecular orbital calculations) the accuracy of the optimised geometry becomes an important point. The calculated HOMA value (Table 1) obtained from HF/3-21G(d) (0.71) is the closest to that obtained by CCSD/6-31G(d) (0.72). The other two Hartree–Fock procedures [using the basis sets 6-31G(d) and 6311 ++G(d,p)] gave results far from the reference value. The variation among the Hartree–Fock calculations excludes them from calculating the physical properties and from the analysis of the structural parameters. The HOMA value obtained by B3LYP/6-31G(d) performed slightly better than the MP2/6-31G(d) method. A similar performance is observed for the **MSB** system (Table 2). Based on these results, B3LYP/6-31G(d) is the most practical.

In light of these results, the ΔE values will be presented for the computational procedures: HF/3-21G(d), B3LYP/6-31G(d) and B3LYP/6-311+G(2d,p)//B3LYP/6-31G(d), and discussing the physical properties will be only based on results obtained from the two B3LYP computational procedures.

3.2 The geometrical parameters

The optimised geometries and the coordinates are available in the supplementary material. The geometries will be discussed based on selected geometrical parameters (Table 3; the enol tautomers, and Table 4; the keto- tautomers). So, what can the geometry tell about the electronic structure?

3.2.1 Structure of the enol-tautomers

The geometry may give a qualitative evaluation of the H-bond strength. Comparatively, the shorter N5···H1 (Table 3) distance means stronger H-bond. The six compounds are arranged according to the strength of the H-bond as the following: **SB-2** > **DH-2** > **H-2** > **SB-1** > **DH-1** > **H-1**. This trend indicates that the basicity of N5 in the naphthalene-based structures (**SB-2**, **DH-2** and **H-2**) is higher than that in the other structures. This means that the former structures include more electron density delocalisation from O1 towards N5 through the OCCCN π-system (Figure 5), which is consistent with our results from previous studies [11,12]. **SB-2** and **SB-1** include stronger H-bonds compared to the analogous hydrazines. In Schiff bases, the higher basicity of N5 is due to bonding to the σ-donor methyl group, while in the hydrazines N5 is bonded to the σ-acceptor N6. One distinguishing feature of the **H-1a** and the **H-2a** geometries is the bond angles H2—N6—N5 (∼109°) and H3—N6—N5 (∼109°), which indicate that the electron pair geometry around N6 is a tetrahedral. This means that the non-bonding electron pair on N6 is weakly conjugated to the NCCCO π-system.

Table 4. Selected structural parameters for the keto-tautomer of the six structures (Figure 2).

Parameter	**SB-1**	**SB-2**	**H-1**	**H-2**	**DH-1**	**DH-2**
N5—H1	1.044	1.036	1.032	1.027	1.045	1.038
O1—H1	1.700	1.716	1.783	1.793	1.734	1.748
O1—C2	1.265	1.260	1.259	1.255	1.262	1.257
C2—C3	1.468	1.464	1.472	1.468	1.473	1.470
C3—C4	1.401	1.397	1.395	1.391	1.392	1.387
C4—N5	1.324	1.329	1.331	1.336	1.335	1.341
H1—N5—C4	111.6	112.5	115.4	116.3	114.3	115.3
H2—N6—N5	–	–	109.4	109.5	–	–
H3—N6—N5	–	–	109.4	109.5	–	–
H3—N6—N5—C4	–	–	63.4	59.3	–	–

Table 5. The HOMA values for the rings and the OCCCN segments.

Compound	Phenyl	OCCCN	
SB-1a	0.91	0.33	
SB-1b	0.42	0.57	
H-1a	0.92	0.30	
H-1b	0.34	0.54	
DH-1a	0.90	0.42	
DH-1b	0.34	0.47	
	Naphthalene		
Compound	Ring A	Ring B	OCCCN
SB-2a	0.836	0.63	0.44
SB-2b	0.88	0.09	0.62
H-2a	0.79	0.65	0.39
H-2b	0.89	0.03	0.58
DH-2a	0.85	0.61	0.54
DH-2b	0.88	0.03	0.56

3.2.2 Structure of the keto-tautomers

Using the same principle, the shorter O1···H1 means stronger H-bond. The H-bond strength in the six structures is arranged as the following: SB-1 > SB-2 > DH-1 > DH-2 > H-1 > H-2 (Table 4). In **DH-1** and **DH-2**, the non-bonding electron pair on N5 can resonate with the second methylidene carbon (Figures 1 and 2), a factor that decreases the electron density contribution towards O1 and makes it less basic which weakens the H-bond with respect to the other structures. In the **H-1** and **H-2** structures, there is a second intramolecular H-bond from the vicinial non-bonding electron pair on N6 with H—N5. Such a side-to-side interaction might be considered as an electrostatic interaction (see the geometries of **H-1** and **H-2** in the supplementary material). This can be deduced also from the change in the values of the dihedral angle H3—N6—N5—C4, its value in the enol-tautomer is 151.6° and changes significantly in the keto-tautomer to become 63.4°. This considerable conformational change indicates that the intramolecular hydrogen bond between N6 and H—N5 is valuable. This characterised vicinal H-bonding is unique and novel, as it appears in the chemical literature, as a significant intramolecular interaction participates in the conformational stability of the keto-tautomers of **H-1** and **H-2**.

3.3 The harmonic oscillator measure of aromaticity

*3.3.1 The phenyl-based structures (**H-1**, **DH-1** and **SB-1**)*

The HOMA values of the phenyl ring in the enol-tautomer (**H-1a**, **DH-1a** and **SB-1a**) are very similar among them (0.91, 0.92 and 0.90, respectively). On the other hand, there are considerable differences among the HOMA values of the OCCCN segments (0.33, 0.30 and 0.42, respectively) (Table 5). This indicates that this part of each of these structures is sensitive to the substituent (—NH_2, —N═CH_2, or —CH_3). In the keto-tautomer, the HOMA values of the phenyl ring changed appreciably; **SB-1b** (0.42), **H-1b** (0.34) and **DH-1b** (0.34), which indicates that the phenyl ring lost a considerable portion of the aromatic character. On the other hand, the HOMA values of the OCCCN segments increased significantly (0.57, 0.54 and 0.47). These values indicate that there is a considerable enhancement of the overlaping among the p-orbitals, which is due to a delocalisation of the non-bonding electron pair of N5 towards O1 (a charge separation). Therefore, the keto-tautomer of these structures is described as zwitterions (Figure 4).

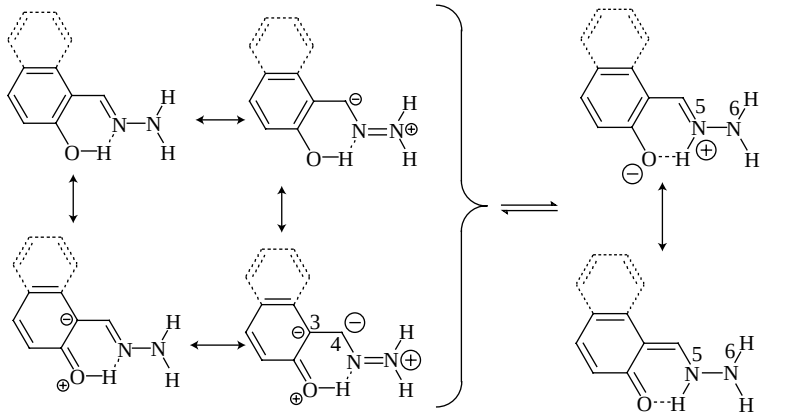

Figure 4. Resonance and the intramolecular electrostatic repulsions that may exist in **H-1** and **H-2**.

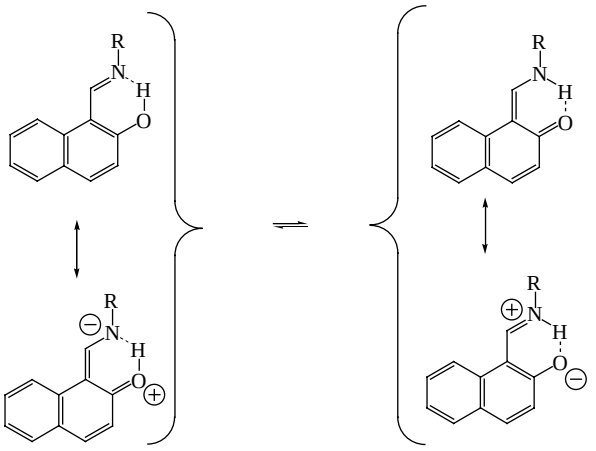

Figure 5. Charge separation in naphthalene-based tautomers.

It is noticed that the HOMA value of the OCCCN segment in **H-1b** (0.54) is higher than that of **DH-1b** (0.47). This is attributed to the presence of a larger intramolecular electrostatic repulsion between the electron densities on the nitrogen atoms N5 and N6 in **H-1b** (Figure 4) compared to **DH-1b**. In **H-1b**, the repulsion is between sp^2 (N5) and sp^3 (N6) orbitals, while in **DH-1b**, the repulsion is less because it is between sp^2 (N5) and another sp^2 (N6) orbital. In addition to that, in **DH-1b** the electron density on N5 is less because of the resonance towards the second methylidene group.

Another interesting observation is that the structure of **SB-1b** has the highest HOMA value (0.57) among the phenyl based structures, which is explained as the following: imagine the structures of **SB-1b**, **H-1b** and **DH-1b** with perfect delocalisation (HOMA = 1) of the lone pair of N5 in the OCCCN π-system, then, there is a positive charge on N5, which is best stabilised by a good σ-donor group; the methyl group in **SB-1b**.

*3.3.2 The naphthalene-based structures (**H-2**, **DH-2** and **SB-2**)*

Ring A in the naphthalene-based systems does not exhibit significant changes in the calculated HOMA values for the enol (**SB-2a**, **DH-2a** and **H-2a**) and the keto (**SB-2b**, **DH-2b**, **H-2b**) tautomers which indicate that the aromatic character remains high nearly unaffected by the tautomerism process. On the other hand, the HOMA values of ring B and the OCCCN segment are similar to the phenyl-based structures (**H-1**, **DH-1** and **SB-1**), they change significantly with the same trend.

It is noticed that the HOMA values of the OCCCN segments in **SB-2**, **DH-2** and **H-2** enol- and keto-tautomers are higher than in **SB-1**, **DH-1** and **H-1**. This means that ring A (**H-2**, **DH-2** and **SB-2**) caused a further enhancement of the overlapping among the p-orbitals. A better overlapping in such a push–pull conjugated system means easier intramolecular charge transfer (separationl; Figure 5) which is the key point in achieving conduction at the molecular and the macromolecular (or polymer) levels [30]. Therefore, structures that can be derived from naphthalene might be better building blocks as electronic materials.

3.4 The energy calculations (ΔE)

The ΔE values may illustrate the significance of substituents on the relative stability of isomers. The data

Table 6. The calculated ΔE (kcal/mol) for the tautomerism process of the six structures (Figure 2) calculated by three computational procedures.

Equilibrium	Computational method	ΔE
H-1a/H-1b	B3LYP/6-31G(d)	11.44
	B3LYP/6-311 +G(2d,p)//B3LYP/6-31G(d)	12.16
	HF/3-21G(d)	10.65
DH-1a/DH-1b	B3LYP/6-31G(d)	6.05
	B3LYP/6-311 +G(2d,p)//B3LYP/6-31G(d)	7.14
	HF/3-21G(d)	8.97
SB-1a/SB-1b	B3LYP/6-31G(d)	3.98
	B3LYP/6-311 +G(2d,p)/B3LYP/6-31G(d)	4.63
	HF/3-21G(d)	5.28
H-2a/H-2b	B3LYP/6-31G(d)	6.30
	B3LYP/6-311 +G(2d,p)//B3LYP/6-31G(d)	7.36
	HF/3-21G(d)	2.71
DH-2a/DH-2b	B3LYP/6-31G(d)	1.49
	B3LYP/6-311 +G(2d,p)//B3LYP/6-31G(d)	2.85
	HF/3-21G(d)	1.71
SB-2a/SB-2b	B3LYP/6-31G(d)	0.33
	B3LYP/6-311 +G(2d,p)//B3LYP/6-31G(d)	0.64
	HF/3-21G(d)	−1.61

Table 7. The selected infrared stretching frequencies (in cm^{-1}) for the enol form of the six structures (Figure 2).

	Enol form		
Structure	C—O	C═N	O—H
H-1a	1325	1689	3365
DH-1a	1335	1709	3243
SB-1a	1337	1720	3165
H-2a	1329	1683	3258
DH-2a	1333	1703	3087
SB-2a	1336	1706	2977

indicate that among the six structures (Figure 2) **H-1** has the largest ΔE (10.65–12.16 kcal/mol). This explains why derivatives of **H-1** have never been reported as thermochromic or photochromic materials. The calculated ΔE of **DH-2**, according to the three computational procedures lay between that for **SB-1** and **SB-2**. Therefore, the derivatives of **DH-2** might be the most promising as molecular materials. By comparing the calculated ΔE values of **H-1** and **H-2** with D**H-1** and **DH-2**, it is obvious that the second methylidene segment caused a decrease in the energy difference between the enol- and the keto-tautomers.

3.5 IR frequencies

The resonance-assisted hydrogen bonding (RAHB) model was first proposed in 1989 [31] to account for the strong intramolecular O—H···O bond occurring in 1,3-diketone enols. It links the H-bond strengthening directly with the enhanced π-delocalisation (p-orbitals overlapping) in the OCCCO segment, which was described later by a number of bonding models [32–34].

As the calculated ΔE (Table 6) predicts dominance of the enol-tautomer, only data for this tautomer are presented and discussed. Table 7 presents the stretching frequencies (in cm^{-1}) of C—O, C═N, and O—H. It is obvious that the C—O and the C═N stretching frequencies in **DH-1a** and **DH-2a** are closer to that in **SB-1a** and **SB-2a**. Based on the RAHB model, this indicates that the delocalisation of the electron density of the OCCCN segment in **DH-1a** and **DH-2a** is closer to that in **SB-1a** and **SB-2a**. This result, again, demonstrates the impact of the second methylidene (Figure 1).

As in the OCCCO, the electron density in the OCCCN π-system is reserved; which implies that a lower O1—H force constant (a lower electron density in the O1—H bond) means a stronger O1—H···N5 H-bond (N5 has more electron density and is more basic), which is consistent with the RAHB model. The variation among the stretching frequencies of the O—H bond indicates that there is also a variation in the basicity of N5, which illustrates the effect of the substituents (on N5) on the total electron density of N5. Based on the O—H stretching frequencies, the force constants of the O—H bond of **DH-1a** and **DH-2a** are closer to that in **SB-1a** and **SB-2a**. The force constant value of **DH-2a** is intermediated between **SB-1a** and **SB-2a**. This similarity of **DH-2a** with **SB-1a** and **SB-2a** was predicted also based on the energy calculations. In general, the IR data support that molecular engineering of **H-1** and **H-2** through introducing the second methylidene group changes the electronic structures to become more similar to the Schiff bases.

3.6 The atomic charges

Since the atomic charge is not a quantum mechanics observation, all methods of computing it are necessarily arbitrary. Of the numerous schemes proposed for atomic population analysis, only Mulliken population analysis has truly found widespread use. The NPA scheme is a more refined wave function-based method that solves most of the problems of the Mulliken scheme by construction of a more appropriate set of (natural) atomic basis functions. The calculation of atomic charges plays an important role in the application of quantum chemical calculations

Table 8. The Mulliken and the NPA charges for the enol tautomer of the six structures (Figure 2).

Structure	H	O1	C2	C3	C4	N5
Mulliken charges						
H-1a	0.437	−0.657	0.298	0.105	0.080	−0.357
DH-1a	0.430	−0.648	0.315	0.088	0.119	−0.397
SB-1a	0.436	−0.652	0.309	0.091	0.102	−0.464
H-2a	0.439	−0.652	0.294	0.019	0.102	−0.379
DH-2a	0.432	−0.642	0.312	0.011	0.133	−0.420
SB-2a	0.438	−0.647	0.307	0.002	0.120	−0.487
NPA charges						
H-1a	0.513	−0.695	0.369	−0.182	0.037	−0.322
DH-1a	0.509	−0.687	0.388	−0.201	0.121	−0.383
SB-1a	0.515	−0.692	0.383	−0.198	0.116	−0.511
H-2a	0.514	−0.691	0.382	−0.177	0.041	−0.328
DH-2a	0.510	−0.682	0.405	−0.195	0.120	−0.390
SB-2a	0.515	−0.687	0.399	−0.194	0.119	−0.521

Table 9. The ^{1}H, ^{13}C, ^{15}N NMR chemical shifts for selected atoms of the enol tautomer of the six structures (Figure 2) calculated using B3LYP/6-311 + G(2d,p)//B3LYP/6-31G(d).

	H	C2	C3	C4	N5
H-1a	11	168	124	152	338
H-2a	12	168	113	148	334
DH-1a	12	171	123	176	369
DH-2a	14	172	113	171	361
SB-1a	13	171	125	173	317
SB-2a	15	172	113	168	307

to molecular systems. They are important in the qualitative rationalisation of organic and inorganic reactivities [35–37]. The nature of this study, being comparative and qualitative, makes it unnecessary to use large basis sets and hence the two schemes Mulliken and NPA were calculated using B3LYP/6-31G(d).

Table 8 presents the computed atomic charges for the OCCCN segment in the six structures. In general, both schemes show a considerable similarity to each other. Oxygen and nitrogen hold negative charges. Simply, the difference in the electronegativities between them explains the higher values on O1. The NPA scheme calculates charges of C3 more consistent with the expected resonance in the O1—C2—C3 segment (Figure 4). In general, the calculated charges using the NPA scheme for H, O1, C2 and C3 in the six structures are similar, which indicates that these parts (the O1—C2—C3 segment) of the molecular structures have similar electron density distribution.

On the other hand, noticeable differences do exist among the calculated charges of the C4═N5 segment, which again brings to attention the importance of the N5 substituents on the electronic structure. The carbon atom C4 in **H-1a** and **H-2a** appears to be nearly neutral which means that the imine group is not a powerful electron-withdrawing group in the presence of the competing electron density pumping from N6 (Figure 4), which explains why the keto-tautomers (**H-1b** and **H-2b**) are not favourable in these cases. In other words, the hydroxyphenyl- and hydroxynaphthyl- groups do not feel a significant electronic effect from the imine group in these two structures.

It is noticed that N5 in **SB-1a** and **SB-2a** has the highest electron density (highest basicity), which explains why these two systems are more prone to form the keto-tautomer compared to the analogous four hydrazine systems. The charge of N5 in **DH-2a** is the closest to that in **SB-1a** and **SB-2a**. Qualitatively, this similarity is consistent with the analysis based on the geometry, the energy calculations and the IR data.

3.7 The ^{1}H, ^{13}C and ^{15}N NMR chemical shifts (δ)

Nuclear magnetic resonance is another method that may allow a direct closer look at the electron density distribution in a molecular structure. The chemical shifts are presented in Table 9. Because of the qualitative nature of this comparison the numbers were rounded without decimal places. The proton chemical shift of **DH-2a** is between that for **SB-1a** and **SB-2a**. The carbon chemical shift of C2 in **DH-1a** and **DH-2a** are closer to that for the two Schiff bases. The chemical shifts of carbon atom C3 may be classified into two groups; compounds derived from phenyl ring (δ; **H-1a** = 124, **DH-1a** = 123, and **SB-1a** = 125) and compounds derived from naphthalene (δ; **H-2a** = 113, **DH-2a** = 113, and **SB-2a** = 113). These values indicate that in the latter group the resonance from O1 to C3 (which creates a negative charge on C3; Figure 4) is more appreciable than that in the phenyl compounds, which is consistent with the HOMA results. The great similarity in the chemical shift values of C3 among the six enol structures indicates that the delocalised electron density in the O1—C2—C3 segment is not affected significantly by the imine (C4—N5-Me) and the hydrazine (C4—N5—N6) segments, which is qualitatively consistent with the NPA results. This piece of information, again, means that the electron density distribution in the O1—C2—C3 segment is very similar among the structures of each group. In addition to that, this means that the point that plays the crucial role in the proton–electron transfer (tautomerism) is the amount of the electron density (basicity) on N5. The carbon atom C4 in **H-1a** and **H-2a** is more shielded compared to the other systems. This result, again, is consistent with the NPA data and with the expected resonance from N6 to C4 (Figure 4).

Shielding of N5 is arranged as the following: **SB-2a** > **SB-1a** > **H-2a** > **H-1a** > **DH-2a** > **DH-1a**. The δ values of N5 in the Schiff bases (N5 is the most shielded; **SB-1a** = 317, **SB-2a** = 307) indicate that the nitrogen has the highest electron density (most basic). This result is qualitatively consistent with the predicted hydrogen bond strength based on the geometrical parameters and the O—H stretching frequencies. Also, this result is qualitatively consistent with the calculated NPA charges (N5 is the most negative/basic; **SB-1a** = −0.511, **SB-2a** = −0.521). It is noticed that the chemical shift values of N5 in **DH-1a** and **DH-2a** are higher (less shielded) than the values of **H-1a** and **H-2a**. This is attributed to the deshielding effect of the neighbouring N6═CH_2 double bond.

3.8 Calculations based on the molecular orbital diagrams

In principle, the molecular orbital diagram might allow even a deeper insight of how molecular engineering based on introducing different substituents might affect the relative stability of certain molecular orbitals which in turn reflects on the overall molecular electronic structure stability. In this section, stability of the keto-tautomers of **H-1**, **H-2**, **DH-1** and **DH-2** will be discussed in light of calculations based on the molecular orbital diagrams.

Table 10. The molecular orbitals that represent the non-bonding electron pairs on N5 and N6 in the keto-tautomers **H-1b**, **H-2b**, **DH-1b** and **DH-2b** based on the B3LYP/6-31G(d) calculations and the ΔE ($|E_{(\text{MO of N6})} - E_{(\text{MOs of N5})}|$).

System	Atom	Molecular orbital number	ΔE (kcal/mol)
H-1b	N6	33	–
	N5	34	27.5
		36 (HOMO)	62.2
H-2b	N6	45	–
	N5	46	9.3
		49 (HOMO)	57.1
DH-1b	N6	36	–
	N5	37	38.0
		39 (HOMO)	70.5
DH-2b	N6	47	–
	N5	49	23.8
		52 (HOMO)	66.5

As was seen in the previous sections, the keto-tautomers **DH-1b** and **DH-2b** are more stable than the keto-tautomers **H-1b** and **H-2b**. In each case, the lone pair located on N6 is represented by one molecular orbital, on the other hand, the lone pair located on N5 is represented by two molecular orbitals. One important piece of information can be extracted from this; the lone pair on N5 is a delocalised electron pair while the lone pair of N6 is a localised electron pair (see the supplementary material for pictures). The absolute values of the energy differences between the molecular orbital of N6 and each of the molecular orbitals of N5 were calculated (Table 10, $\Delta E = |E_{(\text{MO of N6})} - E_{(\text{MOs of N5})}|$). The value obtained for **H-1b** was compared to that obtained for **DH-1b**, and the same was done for the **H-2b** and **DH-2b** pair. It is obvious that in both cases after formation of the second methylidene the energy differences increased. This change is interpreted by saying that the interaction between the two lone pairs became less (after formation of the second methylidene) and therefore it necessarily means that the keto-tautomer in **DH-1** and **DH-2** is more stable than the keto-tautomer in **H-1** and **H-2**. Based on the chemical intuition, this was explained (Section 3.2.3) by looking at the orbitals that hold the N5 and N6 lone pairs; in **H-1b**

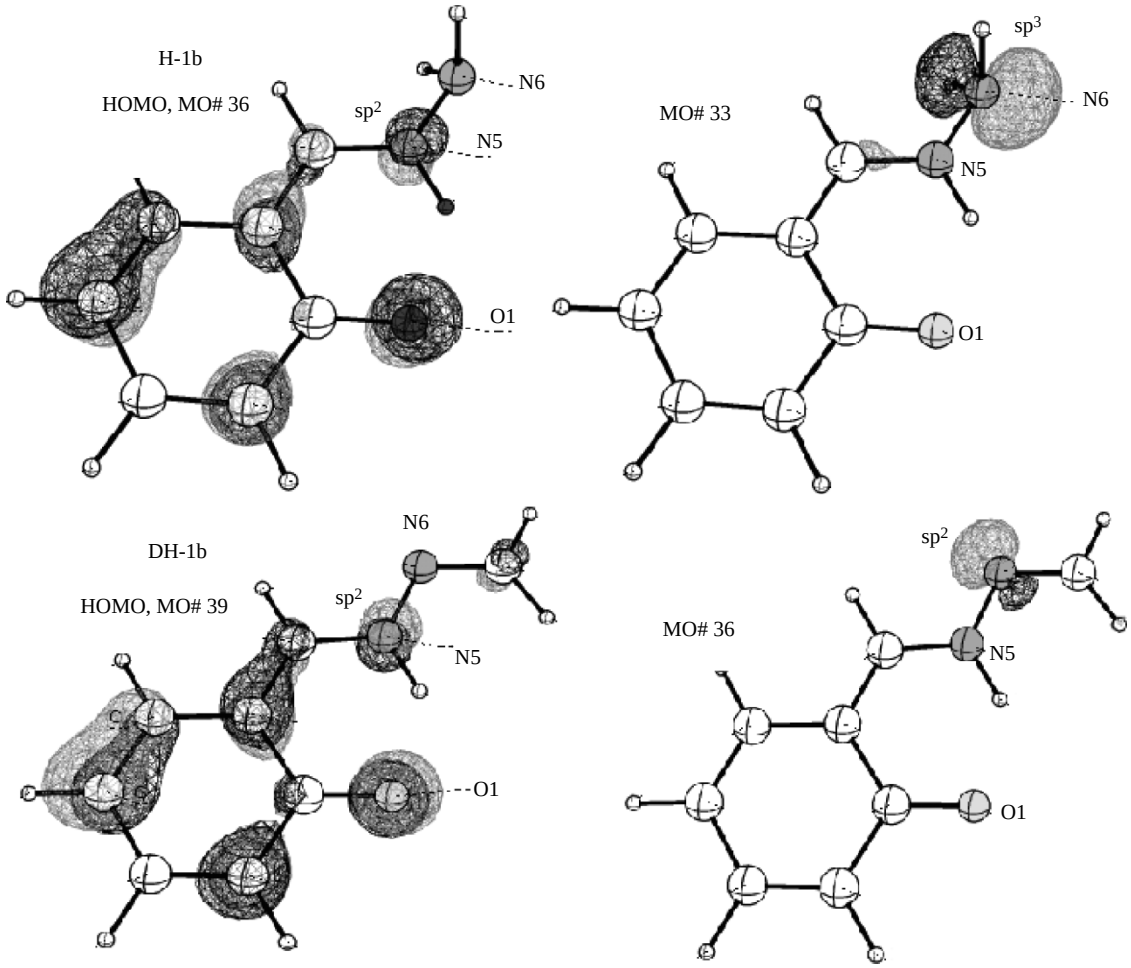

Figure 6. Selected molecular orbitals for **H-1b** and **DH-1b**. See the supplementary material for larger pictures of all the molecular orbitals presented in Table 10.

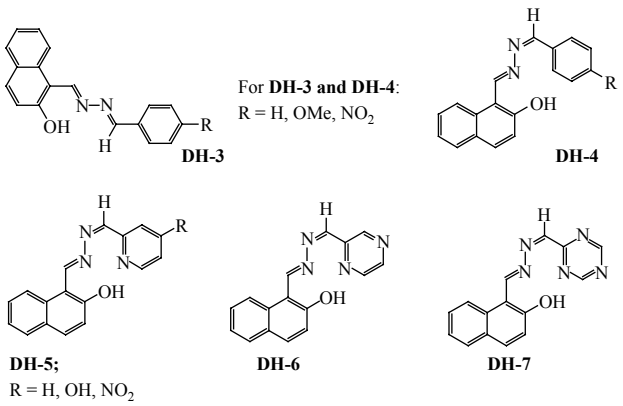

Figure 7. The hydrazines proposed to test effect of R1 and R2 (Figure 2).

and **H-2b** the repulsion is between sp^2 (N5) and sp^3 (N6) orbital which is higher than the repulsion between sp^2 (N5) and sp^2 (N6) orbitals in **DH-1b** and **DH-2b** (Figure 6).

3.9 Effect of R1 and R2

The main purpose of this section is to answer the following question: are the calculated ΔE values (Table 6) the limit for the dimethylidenes hydrazine, in other words, do the substituents on the second methylidene group (Figure 2) affect the proton–electron delocalisation? Based on the previous discussion, the asymmetric hydrazine **DH-2** is the most similar to the Schiff base systems, therefore, it was chosen to test the effect of the substituents. The structures tested in this section are presented in Figure 6. These structures were selected as the following. Analysis of the electronic structure of the Schiff bases and the hydrazines indicate qualitatively that increasing the electron density of N5 is a key point in stabilising the keto-tautomer. This was tested by proposing the two systems **DH-3** and **DH-4** (Figure 7). In addition to this, it was proposed that stabilising the keto-tautomer might be achieved by a π-electron withdrawing group that can stabilise the lone pair of N5 in the keto-tautomer, as in **DH-5**, **DH-6** and **DH-7** (Figure 7).

Before discussing the results, in addition to the very good performance observed for HF/3-21G(d) in predicting the tautomerism position it will be demonstrated that it is an acceptable computational procedure for energy calculations of the isomerisation reaction (tautomerism) at least for qualitative purposes. Cohen [38] studied the thermochromism in anils and calculated the energy difference between the two tautomeric forms. For *N*-(5-chlorosalicylidene)aniline in the solid state, ΔE was found to be a small value; 1.76 kcal/mol. To simulate the effect of the environment in the solid state the packing effect in the crystalline state was neglected and the ΔE was calculated using HF/3-21G(d) (solvent)//HF/3-21G(d) (gas phase)

Table 11. The calculated ΔE (kcal/mol) for the hydrazines in Figure 7 using HF/3-21G(d).

Entry	ΔE	Entry	ΔE
DH-3		**DH-5**	
H	2.55	H	−3.58
OMe	2.63	OH	−3.72
NO_2	2.59	NO_2	−3.13
DH-4			
H	1.33	**DH-6**	−2.91
OMe	1.52	**DH-7**	−2.95
NO_2	1.75		

in polar solvents (e.g. DMSO and THF). The results are close to that calculated experimentally; in DMSO $\Delta E = 1.49$ kcal/mol and in THF $\Delta E = 2.14$ kcal/mol. Qualitatively, the HF/3-21G(d) could predict the ΔE position (+ or −) correctly. The reader should be aware that this recommendation was adopted only for this type of isomerisation, but for other chemical changes a similar evaluation of a variety of methods should be performed to find the suitable computational procedure (time vs. accuracy).

When R1 is a substituted phenyl ring (Figure 7, **DH-3**) the ΔE increased slightly with respect to **DH-2** (Table 11). On the other hand, when the same substituted phenyl ring was placed as R2 (**DH-4**) the ΔE values did not change significantly compared to **DH-2**. The ΔE values of **DH-3** and **DH-4** are not very different from that obtained for **DH-2** which indicates that this type of substitution is not effective in increasing the basicity of N5. The substituted pyridine in **DH-5** caused a significant change in the equilibrium position and the keto-form became the dominant tautomer. The same result was obtained for **DH-6** and **DH-7**. The optimised geometries of **DH-5**, **DH-6** and **DH-7** (see supplementary material) indicate that there is another factor that contributes to the stability of the keto-tautomer which is a second intramolecular hydrogen bond from the hetero-nitrogen in pyridine, pyrazine and triazine.

Substituents on **DH-3** and **DH-4** do not exhibit a certain trend because these substituents are not directly conjugated to N5. On the other hand, the trend in the calculated ΔE of the three **DH-5** derivatives indicates that the hydrogen-bonding from the pyridine hetero-nitrogen is an important factor. It is obvious that this second intramolecular H-bond is stronger when the substituent is a π-donor (the OH group), which is consistent with the general chemical intuition. This result is supported by previous experimental results in which second hydrogen bond was proven to stabilise the keto-tautomer in 1-(quinolin-8-yliminomethyl)-naphthalen-2-ol [39–41]. The supplementary material includes the ΔE values (HF/3-21G(d) for other 14 derivatives of **DH-2** in which there is a second intramolecular H-bond. The results

Figure 8. The enol and the keto-tautomers of the molecular conductor **SB-3** proposed by Inabe for a novel type of molecular electronic devices.

indicate that, in general, the keto-tautomer is more stable. Two proposed approaches were the subject of this section, however, a separate study will be devoted to investigate in more details the factors that may allow to control the proton–electron delocalisation in the hydrazines.

Inabe [42] proposed that in molecular conductors like **SB-3** (Figure 8) charge conduction can be modulated by the proton transfer. If the coupling between the two properties is sufficiently strong, memory or switching functions can be obtained. Thus, by controlling the strength of the coupling, the **SB-3** gives various types of charges conduction, which might be utilised in versatile electronic devices. The calculations have showed that the proton transfer in asymmetric methylidenes hydrazine might be a controllable process. If the asymmetric methylidenes hydrazine in this study might be engineered to pack efficiently and conduct charge in the crystalline form then the charge conduction can be controlled as a function of the substitution. Two important requirements of molecular conductors are available in **DH-3**, **DH-5**, **DH-6** and **DH-7**; the extended conjugation and the planarity which encourages testing them for the molecular electronics applications. The applications related to the tautomersim process have been reported for Schiff bases, but what are the physicochemical features of the methylidenes hydrazine derivatives? The answer remains uncertain, waiting for more research to be carried out in these areas.

4. Conclusion

Evaluating a variety of computational procedures suggested that for qualitative purposes the procedure B3LYP/6-31G(d) is the most practical for calculating the molecular properties. In addition to this method, the computational procedure HF/3-21G(d) produced better tautomerism energies for two model systems based on reference values obtained by CCSD/6-31G(d). Analysing the molecular structures of the six systems using the B3LYP and the HF methods provided with a homogeneous set of information. In general, the calculations illustrated that the hydrazines and the Schiff bases as they switch from the enol- to the keto-tautomer show the same trend in the characteristics of their electronic structures, as predicted in the hypothesis. Regarding the details of the molecular properties of the hydrazines, the analysis revealed that the electrostatic repulsion between the non-bonding electron pair on N6 and the non-bonding electron pair on N5 is the main reason behind destabilising the keto-tautomer in **H-1** and **H-2**. Formation of a second methylidene group decreased this repulsion and stabilised the keto-tautomer. Another important factor that lowered the stability of the keto-tautomer in **H-1**, **H-2**, **DH-1** and **DH-2** with respect to the Schiff bases is the basicity of N5. After understanding the molecular characteristics of the hydrazines with respect to the two Schiff bases two approaches were proposed to investigate the possibility of controlling the proton–electron delocalisation. The first was increasing the basicity of N5 through the second methylidene substituents, which was found unfeasible. However, the second approach, which proved to be effective, includes incorporating a π-acceptor group that can participate also in a second intramolecular hydrogen bonding. This recommendation demonstrated that the tautomerism process (the proton–electron delocalisation) in the hydrazines might be a controllable molecular process. This result opens the door to investigate, experimentally and theoretically, the properties of the wide range of the hydrazines derivatives.

Acknowledgements

Some of the calculations were performed using the computational chemistry facilities at the New Mexico State University, USA, special thanks are due to Dr H. Wang. Also, we thank Al-Hussein Bin Talal University for the generous support through the research grant 2008/78.

References

[1] E. Hadjoudis and I.M. Mavridis, *Photochromism and thermochromism of Schiff bases in the solid state: structural aspects*, Chem. Soc. Rev. 33 (2004), pp. 579–588.
[2] B.L. Feringa, W.F. Jager, and B. DeLange, *Organic materials for reversible optical data storage*, Tetrahedron 37 (1993), pp. 8267–8310.
[3] K. Amimoto and T. Kawato, *Photochromism of organic compounds in the crystal state*, J. Photochem. Photobiol. C: Photochem. Rev. 6 (2005), pp. 207–226.
[4] E. Hadjoudis, M. Vittorakis, and I. Moustakali-Mavridis, *Photochromism and thermochromism of Schiff bases in the solid state and in rigid glasses*, Tetrahedron 43 (1987), pp. 1345–1360.
[5] H. Durr and H. Bouas-Laurent, *Photochromism: Molecules and Systems*, Elsevier, Amsterdam, 1990.
[6] Y. Zhang and Z.H. Lu, *A multi-component molecular material design study on the correlation of electronic properties and proton transfer in* N-*salicylideneaniline derivatives*, Mater. Chem. Phys. 63 (2000), pp. 188–195.
[7] Y. Zhang and Z.H. Lu, *A theoretical study on* N,N′*-disalicylidene-p-phenylenediamine (BSP) for the multi-component material design,* Mater. Chem. Phys. 57 (1999), pp. 253–259.
[8] D. Ginsburg, *Solid State Photochemistry*, Verlag Chemie, New York, 1976.
[9] A. Sytnik and J.C. Del Valle, *Steady-state and time-resolved study of the proton-transfer fluorescence of 4-hydroxy-5-azaphenanthrene in model solvents and in complexes with human serum albumin*, J. Phys. Chem. 99 (1995), pp. 13028–13032.
[10] S.J. Isak, E.M. Eyrimg, J.D. Spikes, and P.A. Meekins, *Direct blue dye solutions: photo properties*, J. Photochem. Photobiol. A 134 (2000), pp. 77–85.

[11] T. Irshaidat, *A DFT study on the mono lithium and sodium salts of N-(2-hydroxyphenyl)salicylaldimine*, Tetrahedron Lett. 50 (2009), pp. 825–830.
[12] T. Irshaidat, *Some physical organic aspects of salicylaldehydes oximes, a theoretical study*, Tetrahedron Lett. 49 (2008), pp. 631–635.
[13] J. Kruszewski and T.M. Krygowski, *Definition of aromaticity basing on the harmonic oscillator model*, Tetrahedron Lett. 36 (1972), pp. 3839–3842.
[14] T.M. Krygowski, *Crystallographic studies of inter- and intramolecular interactions reflected in aromatic character of pi-electron systems*, J. Chem. Inf. Comput. Sci. 33 (1993), pp. 70–78.
[15] T.M. Krygowski and M.K. Cyrański, *Structural aspects of aromaticity*, Chem. Rev. 101 (2001), pp. 1385–1419.
[16] A.D. Becke, *Density-functional thermochemistry. III. The role of exact exchange*, J. Chem. Phys. 98 (1993), pp. 5642–5648.
[17] C. Lee, W. Yang, and R.G. Parr, *Development of the Colle–Salvetti correlation-energy formula into a functional of the electron-density*, Phys. Rev. B 37 (1988), pp. 785–789.
[18] W.J. Hehre, R. Ditchfield, and J.A. Pople, *Self-consistent molecular orbital methods. XII. Further extensions of Gaussian-type basis sets for use in molecular orbital studies of organic molecules*, J. Chem. Phys. 56 (1972), pp. 2257–2261.
[19] M.J. Frisch, G.W. Trucks, H.B. Schlegel, G.E. Scuseria, M.A. Robb, J.R. Cheeseman, J.A. Montgomery, T. Vreven, K.N. Kudin, J.C. Burant, J.M. Millam, S.S. Iyengar, J. Tomasi, V. Barone, B. Mennucci, M. Cossi, G. Scalmani, N. Rega, G.A. Petersson, H. Nakatsuji, M. Hada, M. Ehara, K. Toyota, R. Fukuda, J. Hasegawa, M. Ishida, T. Nakajima, Y. Honda, O. Kitao, H. Nakai, M. Klene, X. Li, J.E. Knox, H.P. Hratchian, J.B. Cross, C. Adamo, J. Jaramillo, R. Gomperts, R.E. Stratmann, O. Yazyev, A.J. Austin, R. Cammi, C. Pomelli, J.W. Ochterski, P.Y. Ayala, K. Morokuma, G.A. Voth, P. Salvador, J.J. Dannenberg, V.G. Zakrzewski, S. Dapprich, A.D. Daniels, M.C. Strain, O. Farkas, D.K. Malick, A.D. Rabuck, K. Raghavachari, J.B. Foresman, J.V. Ortiz, Q. Cui, A.G. Baboul, S. Clifford, J. Cioslowski, B.B. Stefanov, G. Liu, A. Liashenko, P. Piskorz, I. Komaromi, R.L. Martin, D.J. Fox, T. Keith, M.A. Al-Laham, C.Y. Peng, A. Nanayakkara, M. Challacombe, P.M.W. Gill, B. Johnson, W. Chen, M.W. Wong, C. Gonzalez, and J.A. Pople, *Gaussian 03, Revision A. 1*, Software available from Gaussian, Inc., Pittsburgh, PA, 2003.
[20] A.E. Reed, L.A. Curtiss, and F. Weinhold, *Intermolecular interactions from a natural bond orbital, donor–acceptor viewpoint*, Chem. Rev. 88 (1988), pp. 899–926.
[21] R.S. Mulliken, *Criteria for the construction of good self-consistent-field molecular orbital wave functions, and the significance of LCAO-MO population analysis*, J. Chem. Phys. 36 (1962), pp. 3428–3439.
[22] R. McWeeny and G. Dierksen, *Self-consistent perturbation theory. II. Extension to open shells*, J. Chem. Phys. 49 (1968), pp. 4852–4856.
[23] S. Saebo and J. Almlof, *Avoiding the integral storage bottleneck in LCAO calculations of electron correlation*, Chem. Phys. Lett. 154 (1989), pp. 83–89.
[24] R. Krishnan and J.A. Pople, *Approximate fourth-order perturbation theory of the electron correlation energy*, Int. J. Quant. Chem. 14 (1978), pp. 91–100.
[25] E.A. Salter, G.W. Trucks, and R.J. Bartlett, *Analytic energy derivatives in many-body methods. I. First derivatives*, J. Chem. Phys. 90 (1989), pp. 1752–1766.
[26] G.E. Scuseria and H.F. Schaefer III, *Is coupled cluster singles and doubles (CCSD) more computationally intensive than quadratic configuration interaction (QCISD)?*, J. Chem. Phys. 90 (1989), pp. 3700–3703.
[27] K.D. Dobbs and W.J. Hehre, *Molecular orbital theory of the properties of inorganic and organometallic compounds. 6. Extended basis sets for second-row transition metals*, J. Comp. Chem. 8 (1987), pp. 880–893.
[28] M.P. McGrath and L. Radom, *Extension of Gaussian-1 (G1) theory to bromine-containing molecules*, J. Chem. Phys. 94 (1991), pp. 511–516.
[29] K. Wolinski, J.F. Hilton, and P. Pulay, *Efficient implementation of the gauge-independent atomic orbital method for NMR chemical shift calculations*, J. Am. Chem. Soc. 112 (1990), pp. 8251–8260.
[30] E.V. Anslyn and D.A. Dougherty, *Modern Physical Organic Chemistry*, University Science Books, Sausalito, CA, 2004.
[31] V. Bertolasi, P. Gilli, V. Ferretti, and G. Gilli, *Evidence for resonance-assisted hydrogen bonding. 2. Intercorrelation between crystal structure and spectroscopic parameters in eight intramolecularly hydrogen bonded 1,3-diaryl-1,3-propanedione enols*, J. Am. Chem. Soc. 113 (1991), pp. 4917–4925.
[32] P. Gilli, V. Bertolasi, V. Ferretti, and G. Gilli, *Covalent versus electrostatic nature of the strong hydrogen bond: discrimination among single, double, and asymmetric single-well hydrogen bonds by variable-temperature X-ray crystallographic methods in β-diketone enol RAHB systems*, J. Am. Chem. Soc. 126 (2004), pp. 3845–3854.
[33] C. Gatti, F. Cargnoni, and L. Bertini, *Chemical information from the source function*, J. Comput. Chem. 24 (2003), pp. 422–436.
[34] S.J. Grabowski, A.T. Dubis, D. Martynowski, M. Glowka, M. Palusiak, and J. Leszczynski, *Crystal and molecular structure of pyrrole-2-carboxylic acid; π-electron delocalization of its dimers – DFT and MP2 calculations*, J. Phys. Chem. A 108 (2004), pp. 5815–5822.
[35] F. Jensen, *Introduction to Computational Chemistry*, Wiley, New York, 1999.
[36] C.J. Cramer, *Essentials of Computational Chemistry*, Wiley, New York, 2002.
[37] J. Cioslowski, *Encyclopedia of Computational Chemistry*, Wiley, New York, 1988.
[38] M.D. Cohen, G.M.J. Schmidt, and S. Flavian, *Topochemistry. Part VI. Experiments on photochromy and thermochromy of crystalline anils of salicylaldehydes*, J. Chem. Soc. (1964), pp. 2041–2051.
[39] F. Esmadi and T. Irshaidat, *Double bond transfer in 2-hydroxyl-1-naphthalidine-8-aminoquinoline and some of its nickel(II) complexes*, Can. J. Anal. Sci. Spect. 44 (1999), pp. 114–119.
[40] K.A. Abbas, S.R. Salman, S.M. Kanan, and Z.A. Fataftah, *Tautomerism in naphthyl amine Schiff bases*, Can. J. Appl. Spectrosc. 41 (1996), pp. 119–124.
[41] P. Fita, E. Luzina, T. Dziembowska, D. Kopec, P. Piatkowski, Cz. Radzewicz, and A. Grabowska, *Keto–enol tautomerism of two structurally related Schiff bases: direct and indirect way of creation of the excited keto tautomer*, Chem. Phys. Lett. 416 (2005), pp. 305–310.
[42] T. Inabe, *New Schiff base molecular conductors*, New J. Chem. 15 (1991), pp. 129–136.